# Origin of ferromagnetism of $MnSi_{1.7}$ nanoparticles in Si: First-principles calculations

Shin Yabuuchi,[1,2] Hiroyuki Kageshima,[1,*] Yukinori Ono,[1] Masao Nagase,[1] Akira Fujiwara,[1] and Eiji Ohta[2]
[1]*NTT Basic Research Laboratories, NTT Corporation, 3-1 Morinosato-Wakamiya, Atsugi, Kanagawa 243-0198, Japan*
[2]*Department of Applied Physics and Physico-Informatics, Keio University, 3-14-1 Hiyoshi, Kouhoku, Yokohama, Kanagawa 223-8522, Japan*

(Received 10 April 2008; revised manuscript received 12 June 2008; published 11 July 2008)

The origin of the magnetism of $MnSi_{1.7}$ nanoparticles in Si is investigated using the first-principles calculations: bulk and interface effects are considered. The bulk magnetic property is expected to be affected by stoichiometry, strain, and charge accumulation. Stoichiometry and charge accumulation induce a ferromagnetic state, and strain stabilizes the ferromagnetic state. Another factor, the $MnSi_{1.7}$/Si interface formation, is seen as triggering ferromagnetism strongly localized at the interface. These two mechanisms are shown to be related to the experimentally determined hard and soft components, respectively.

DOI: 10.1103/PhysRevB.78.045307 PACS number(s): 75.50.Pp, 75.70.Cn, 63.20.dk, 71.20.−b

## I. INTRODUCTION

Controlling the spin degrees of freedom is a challenging topic in physics as well as in engineering.[1,2] In particular, silicon (Si)-based spintronics is of great importance because it is expected to open a new field in physics with its combination with highly advanced silicon electronics technologies.[3–5]

Recently, room-temperature ferromagnetism was reported for manganese (Mn)-ion implanted Si (Ref. 6). The Curie temperature has been evaluated to be over 400 K. The ferromagnetic properties are reported to be affected by the Mn concentration, the thermal annealing process, and the carrier type of the Si substrate. The diluted magnetic semiconductor is suggested to be the origin of the magnetic property because the carriers seem to mediate the ferromagnetism. However, the transition metals, such as Mn, are known to have very low solubility in Si and easily react with Si to form silicides.[7–9] It has been reported that the manganese-silicide $MnSi_{1.7}$ nanoparticles in Si exhibit ferromagnetism with a relatively large magnetic moment.[10]

We have experimentally investigated the temperature-dependent magnetic properties of manganese-silicide $MnSi_{1.7}$ nanoparticles in Si by controlling the particle diameter from 3 to 26 nm (Ref. 11). We have demonstrated that the saturation magnetization and the coercivity change with the temperature and particle size. From a deep analysis that included the switching field distribution technique, we concluded that the ferromagnetism is consists of two components, hard and soft, and that the hard component offers coercivity values as high as 2500 Oe.

It is not clear, however, what the origins of the ferromagnetism are. $MnSi_{1.7}$ belongs to a family of compounds known as Nowotny chimney-ladder phases.[12,13] $MnSi_{1.7}$ is known to have many phases such as $Mn_4Si_7$, $Mn_{11}Si_{19}$, $Mn_{15}Si_{26}$, $Mn_{26}Si_{45}$, and $Mn_{27}Si_{47}$.[14–20] Previous experimental or computational studies of bulk (not nanoscaled) $MnSi_{1.7}$ (Refs. 20–24) do not give a sufficient explanation for the ferromagnetism of the $MnSi_{1.7}$ nanoparticles/Si system. This suggests the importance of strain, charge transfer, etc. that could be induced in the nanoparticles. The particle size and/or the interface formation could also play an important role in determining the magnetism.

This work rectifies this omission by introducing a systematic study based on the first-principles calculations that addresses the physical origin of the ferromagnetism of $MnSi_{1.7}$ nanoparticle/Si system. We focus on the effects of strain, charge transfer, and interface formation on the magnetic properties of $MnSi_{1.7}$.

## II. METHOD

The calculation method used in this work follows the work used in the previous report.[25,26] The first-principles calculations performed are based on the density-functional theory within the generalized gradient approximation (GGA) and the local spin-density (LSD) (Ref. 27) approximation. We use the Vanderbilt ultrasoft pseudopotential[28,29] for Mn and the Troullier-Martins pseudopotential[30] for Si. The pseudopotential of Mn is built with the electronic configurations of $3d^6$, $4s^1$, $4p^0$, and the cut-off radius of $r_c$=2.5 a.u. We also apply the plane-wave basis setup to the cutoff of 25 Ry and fully optimize the atomic configurations before evaluating their magnetic moments. The $k$-point sampling is $4\times4\times4$ for $Mn_4Si_7$ and $4\times4\times2$ for $Mn_{11}Si_{19}$ in the first Brillouin zone. All calculations are done with TAPP (Tokyo Ab-initio Program Package), which we developed.[31–33]

We first examine bulk Si and cubic MnSi in order to check the accuracy of the pseudopotentials used in the calculation. For bulk Si, the calculated lattice constant is 5.46 Å, which is well consistent with the experimental value of 5.43 Å (0.6% error). For bulk MnSi, the calculated lattice constant is 4.58 Å, which is also well consistent with the experimental value of 4.558 Å (Ref. 34) (0.5% error). The calculated magnetic moment for bulk MnSi is 0.9 $\mu_B$, which closely matches the previous calculated value of 0.4 $\mu_B$ at the lattice constant of 4.44 Å (Ref. 35).

$Mn_4Si_7$ has a tetragonal space group $P\bar{4}c2$ with lattice constants $a$=5.5259 Å and $c$=17.5156 Å (Ref. 20) as shown in Fig. 1(a). It is consists of the subcells of Mn [Fig. 1(d)] and a helical arrangement of Si [Fig. 1(e)]. Considering symmetry, the 16 Mn atoms in the unit cell are classified into five groups, which are placed at position Mn1 (0,0,0), Mn2 (1/2,0,0.06508), Mn3 (1/2,1/2,0.12939), Mn4 (0,1/2,0.19137), and Mn5 (0,0,1/4) as shown in Fig. 1(b). The

 

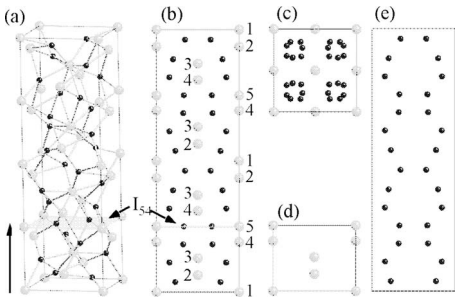


FIG. 1. Atomic images of (a) unit cell, (b) side view, (c) top view, (d) Mn subcell, and (e) Si arrangement, of $Mn_4Si_7$ crystal. The large and small circles are Mn and Si atoms, respectively. The numbers shown in (b) indicate the symmetry type of Mn atoms. $I_{54}$ indicates one of the (001) planes.

plane perpendicular to the $c$ axis that includes Mn atoms can be defined as $I_{xy}$, where $x$ and $y$ are the indices of the Mn atom as shown in Fig. 1(b). For bulk $Mn_4Si_7$, the calculated lattice constant $a$ is 5.55 Å, which agrees well with the experimental value (0.5% error). The estimated bulk modulus of $Mn_4Si_7$ is 1.87 Mbar.

$Mn_{11}Si_{19}$ has a tetragonal space group $P\bar{4}n2$ with lattice constants $a$=5.52 Å and $c$=48.2 Å (Ref. 19). Its crystal structure resembles with that of $Mn_4Si_9$ except for the periodicity along the $c$ axis. For bulk $Mn_{11}Si_{19}$, the calculated lattice constant $a$ is 5.54 Å, which agrees well with the experimental value. The estimated bulk modulus of $Mn_{11}Si_{19}$ is 1.88 Mbar, which coincides with that of $Mn_4Si_7$.

## III. BULK MAGNETIC PROPERTIES

We first calculate the band structures and the DOS of bulk $Mn_4Si_7$ and the $Mn_{11}Si_{19}$. For $Mn_4Si_7$, the Fermi energy is located in the band gap. The gap width is 0.8 eV [Fig. 2(a)]. These results are consistent with the previous theoretical reports.[21,22] We then take account of the spin polarization to investigate the magnetic properties, but magnetism does not appear due to its semiconductorlike band structure. $Mn_4Si_7$ is thus an intrinsic semiconductor and is a nonmagnetic material.

For $Mn_{11}Si_{19}$, the Fermi energy is located just below the valence-band top [Figs. 2(b)–2(d)]. It should be noted that the calculated band structures of $Mn_4Si_7$ and $Mn_{11}Si_{19}$ are quite similar except for the Fermi energy position. These results are also consistent with the previous theoretical reports.[21,22] Next, we take account of the spin polarization but again magnetism does not appear.

As shown in Fig. 2(d), the DOS is very large just below and above the band gap because the bands around here are mainly due to the $d$ orbitals of the Mn atoms. Such a characteristic is also seen in $Mn_4Si_7$. The large DOS around the Fermi energy could cause the ferromagnetic ordering. We therefore calculate the relationship between the total energy and the spin polarization to evaluate the stability of the ferromagnetic ordering.

The filled circles in Fig. 3 show the total energy difference as a function of the occupancy difference between the

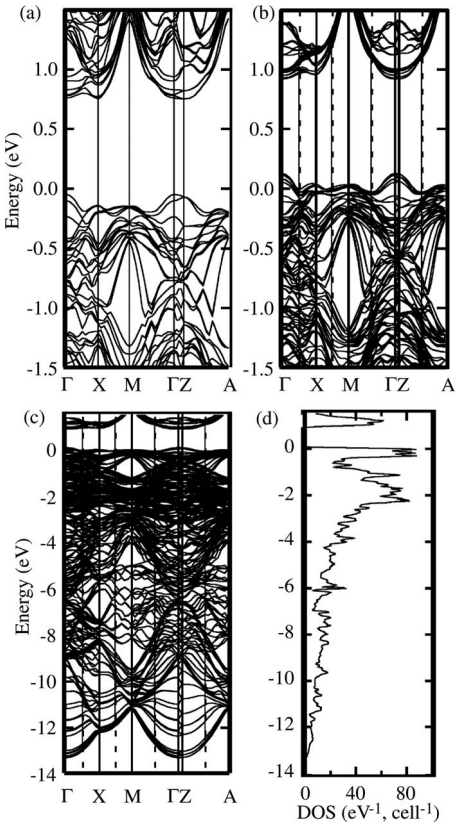


FIG. 2. Calculated band dispersion relations of (a) bulk $Mn_4Si_7$ and (b)–(c) bulk $Mn_{11}Si_{19}$. (d) Calculated density of states (DOS) of bulk $Mn_{11}Si_{19}$. The region near the Fermi energy is closed up in (a) and (b). Energy zero corresponds to the Fermi energy in all figures.

up-spin and the down-spin states, $N_{up}-N_{down}$. As shown in the figure, $Mn_{11}Si_{19}$ is assuredly a nonmagnetic material because the nonmagnetic state, $N_{up}-N_{down}=0$, is the most stable arrangement. However, a metastable ferromagnetic state appears at $|N_{up}-N_{down}|=4$. The calculated band structure of the metastable ferromagnetic state indicates that the Fermi energy is located in the band gap for the up-spin state while it is located in the valence band below the band gap for

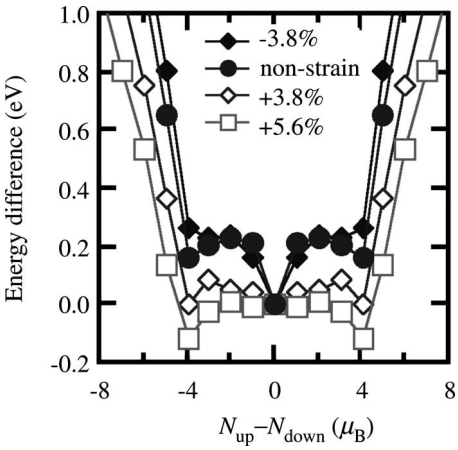


FIG. 3. The strain effects on the total energy difference of $Mn_{11}Si_{19}$ as a function of the occupation difference between the up-spin and the down-spin states, $N_{up}-N_{down}$.

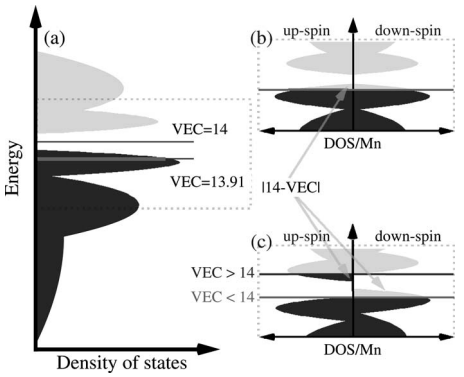


FIG. 4. Schematic picture of (a) DOS for nonmagnetic $MnSi_{1.7}$, (b) the partial DOS of the up- and down-spin states for nonmagnetic $MnSi_{1.7}$, and (c) the partial DOS of the up-spin and down-spin states for ferromagnetic (half metallic) $MnSi_{1.7}$. The horizontal lines indicate the Fermi energy positions.

the down-spin state. All Mn atoms are slightly polarized and have some magnetic moment, while each Mn atom has a different polarized electron density. The value of the averaged magnetic moment is very weak, only 0.09 $\mu_B$/Mn. This means that $Mn_{11}Si_{19}$ could be half metallic in its metastable ferromagnetic state and that its magnetism can be classed as itinerant ferromagnetism.

These results suggest that magnetic properties of $MnSi_{1.7}$ are easily affected by changes in stoichiometry. Such a dependency can be explained by the theory for chimney-ladder compounds, usually referred to as the valence electron concentration (VEC), the number of valence electrons per transition metal atom.[36–38] The theory is also referred to as the 14-electron rule. VEC can be calculated as $VEC=7+4\times y/x$ for Mn-silicide $Mn_xSi_y$, since Mn and Si have seven and four valence electrons, respectively. The validity of this VEC theory for $Mn_4Si_7$ and $Mn_{11}Si_{19}$ has already verified[22] and is also supported by our results. The VEC theory predicts that compounds with the VEC of 14 are semiconductors and that the valence-band occupation of those compounds is determined by just VEC. Figure 4 shows schematics of the relationship between the DOS of $MnSi_{1.7}$ and electron occupation.

The VEC theory thus predicts the magnetic properties of this material. The mechanism of magnetism is considered to be similar to that of transition metals such as Ni or Pd, where a part of the electrons in the localized *d* band transfers to the free-electronlike *s*-band and holes are doped in the *d* band. A consideration of the classical Stoner theory with regard to the itinerant magnetism of such transition metals suggests that ferromagnetism will occur when the Stoner criterion $D(E_F)\times I>1$ is satisfied, where $I$ is the exchange integral and $D(E_F)$ is the DOS at the Fermi energy.[39] According to the more sophisticated Kanamori theory, which considers multiple scattering, the Stoner criterion should be modified to $D(E_F)\times U_{eff}>1$, where $U_{eff}$ is the effective exchange energy.[40] In both cases, a large DOS at the Fermi energy is necessary for ferromagnetism.

When VEC decreases from 14, the system becomes hole-doped semiconductorlike and the DOS at the Fermi energy increases rapidly. The increase in the DOS enhances the correlation between the carriers, and the ferromagnetic ordering should become more stable. Among the various phases of $MnSi_{1.7}$, $Mn_{11}Si_{19}$ has the lowest VEC, 13.91, and the largest DOS at the Fermi energy, suggesting that it could be the dominant cause of the appearance of ferromagnetism. The averaged magnetic moment of our metastable ferromagnetic $Mn_{11}Si_{19}$, 4/44=0.09 $\mu_B$/Mn, agrees well with the difference between 14 and VEC, 14−VEC=0.09, which corresponds to the unit density of the doped carriers in the *d* orbital originated valence band per Mn atom (Table I). These discussions suggest that the magnetism of the $MnSi_{1.7}$ nanoparticles in Si would also strongly depend on the stoichiometry of the particle and the ferromagnetism is expected to be strongest when the particle is $Mn_{11}Si_{19}$ but note that the stability of the ferromagnetism does not seem to be sufficient.

TABLE I. Relation of crystal phase of the $MnSi_{1.7}$, corresponding *c*-axis lattice constant, value of valence electron concentration (VEC), and maximum magnetic moment estimated from the VEC theory.

| | *c* axis (nm)[a] | VEC | $M_{max}^{VEC}$ |
|---|---|---|---|
| $Mn_4Si_7$ | 1.75 | 14 | 0 |
| $Mn_{11}Si_{19}$ | 4.82 | 13.91 | 0.09 |
| $Mn_{15}Si_{26}$ | 6.53 | 13.93 | 0.07 |
| $Mn_{26}Si_{45}$ | 11.34 | 13.92 | 0.08 |
| $Mn_{27}Si_{47}$ | 11.79 | 13.96 | 0.04 |

[a]Reference 19.

## IV. STRAIN AND CHARGING EFFECTS

In the experiments, nanoparticles are buried in the host silicon. This suggests that the strain and/or the charge transfer is induced in the particles and causes the ferromagnetism. First we examine the strain effect. For $Mn_4Si_7$, isotropic tensile (compressive) strain narrows (widens) the band gap. No ferromagnetism appears in the range between 4% tensile strain and 4% compressive strain. On the other hand, for $Mn_{11}Si_{19}$, isotropic tensile strain can stabilize the ferromagnetic state. Figure 3 shows the total energy difference as a function of the occupancy difference between the up-spin and the down-spin states at each strain for $Mn_{11}Si_{19}$. As shown in the figure, isotropic tensile strain stabilizes the metastable ferromagnetic state. Finally the ferromagnetic state becomes most stable when the applied tensile strain is 5.6%. Here we note that the magnetic moment of the ferromagnetic state, $|N_{up}-N_{down}|=4$, is independent of the tensile strain.

Next we investigate the impact of charge accumulation on the magnetism of $Mn_4Si_7$. Figure 5 shows the total energy difference as a function of the occupancy difference between the up-spin and the down-spin states at each charging case. In the neutral case, no metastable state appears. When charge is accumulated, the metastable ferromagnetic state appears and becomes stable at large absolute values of the accumulated charge regardless of the polarity of the charge. The figure also indicates that the magnetic moment of the ferro-

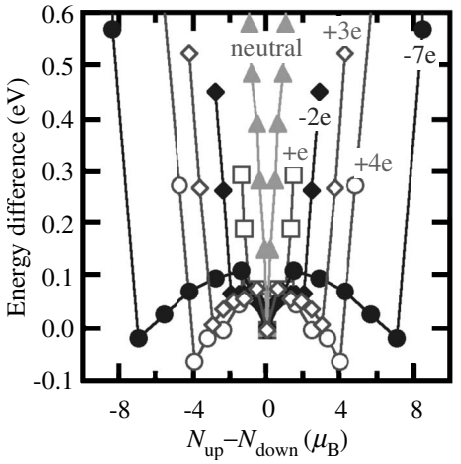


FIG. 5. Total energy difference of $Mn_4Si_7$ as a function of the occupation difference of the up-spin and the down-spin states. Open circles, open diamonds, and open squares indicate hole-doped cases with the density of +4/cell, +3/cell, and +1/cell, respectively. Closed circles and closed diamonds indicate electron-doped cases with the density of −7/cell and −2/cell, respectively. Closed triangle indicates neutral case.

magnetic state, $M_{max}^{FM}=|N_{up}-N_{down}|/16$, increases with the absolute value of the accumulated charge.

The VEC theory is useful in discussing these results. It is expected that applying strain would change only the DOS but not the Fermi energy position. Since $Mn_4Si_7$ has semiconductor nature, strain should not induce any ferromagnetism. On the other hand, since $Mn_{11}Si_{19}$ has hole-doped semiconductor nature and the Fermi energy is located in the *d* orbital originated valence band, the application of tensile strain could more strongly localize the *d* orbitals, enhance the DOS at the Fermi energy, and stabilize the ferromagnetic states.

The shift of the Fermi energy position due to charge accumulation can be interpreted as a change in VEC. VEC decreases with hole accumulation and increases with electron accumulation. In both cases, the DOS at the Fermi energy should increase and ferromagnetism should be induced [Fig. 4(c)] with the magnetic moment of $M_{max}^{VEC}=|14-VEC|$. The relationship between the accumulated charge and effective VEC is shown in Table II. As shown in the table, the magnetic moments yielded by the first-principles calculation well match those obtained from VEC. This also means that all accumulated additional charges are, in total, the source of the ferromagnetism.

These calculated results clearly indicate that the tensile strain can certainly enhance the stability of the ferromagnetism and that the charge accumulation can enhance the magnetic moments of the ferromagnetism. The ferromagnetism induced by these effects is, however, considered as the itinerant magnetism with the magnetic moment just around 0.01–0.1 $\mu_B$/Mn, if we consider the realistic stoichiometry changes or charge accumulation. Since either the strain or the charge accumulation does not change the electronic state with the hole-doped *d* band, they cannot change the origin of the ferromagnetism of the $MnSi_{1.7}$, either. To explain the two component ferromagnetism found in the nanoparticle experiments, another cause of the ferromagnetism is necessary.

TABLE II. Relation of accumulated charges, magnetic moment estimated from the calculated occupation difference of the ferromagnetic state, $M_{max}^{FM}=|N_{up}-N_{down}|/16$, the stability of the calculated ferromagnetic states, effective VEC estimated from accumulated charge, and maximum magnetic moment evaluated from the VEC theory. Bulk $Mn_4Si_7$ case shown in Fig. 5.

| Charge/cell | $M_{max}^{FM}$ | Stabilility | VEC | $M_{max}^{VEC}$ |
|---|---|---|---|---|
| −7 | 0.44 | stable | 14.44 | 0.44 |
| −2 | 0.13 | metastable | 14.13 | 0.13 |
| 0 | 0.00 | stable | 14.00 | 0.00 |
| 1 | 0.06 | metastable | 13.94 | 0.06 |
| 4 | 0.25 | stable | 13.75 | 0.25 |

## V. INTERFACE EFFECT

When the $MnSi_{1.7}$ nanoparticles are formed in Si, an interface with the host Si matrix is created and may play an important role in the magnetic properties. This can be expected as another cause of the nanoparticle ferromagnetism. Thus, we investigate the magnetism of $MnSi_{1.7}$/Si interfaces by the first-principles calculation.

We prepare the interface models as follows: As shown in Sec. II, Mn atoms in $Mn_4Si_7$ can be classified into five groups and the (001) plane is into eight groups according to crystal symmetry (Fig. 1). Therefore, the interfaces can be denoted as $I_{xy}$ ($I_{12}$, $I_{23}$, etc.), where the index of the Mn layer closest to the interface is *x* and that of the second closest is *y*. We first cut $Mn_4Si_7$ crystal at the $I_{45}$ plane and simply put a Si(001) slab on the resulting surface. Then we introduced Mn atoms into the interface to grow the $Mn_4Si_7$(001) slab and we formed seven different interfaces from $I_{54}$ to $I_{34}$. The initial Si slab has eight Si atomic layers and the initial $Mn_4Si_7$ slab has four Mn atomic layers. We employed the superslab geometry with a sufficiently thick vacuum layer and hydrogen-terminated surfaces. Among the various interface arrangements possible between Si(001) and $Mn_4Si_7$(001), we found that magnetism appears on particular metallic interfaces, while semiconducting interfaces and other metallic interfaces were nonmagnetism (Fig. 6).

Figure 7 shows the cross-sectional atomic configuration of one of the magnetic interface $I_{54}$, its spin polarized electron densities and the difference in electron density. The electron density is polarized only around the interfacial Mn atoms as shown in Fig. 7(d). The thickness of the spin polarized region is about 0.3–0.5 nm. The electron density is not polarized around the Mn atoms further from the interface. Thus, the magnetic moment of the interfacial Mn is $\sim 1\mu_B$/Mn, which is larger than that for the bulk $MnSi_{1.7}$ (see previous sections).

In bulk $Mn_4Si_7$, all the 3*d* orbitals of a Mn atom contribute to the chemical bonds with Si, which results in the semiconducting and nonmagnetic nature. However, the atomic density and the coordination number of Mn at the interface

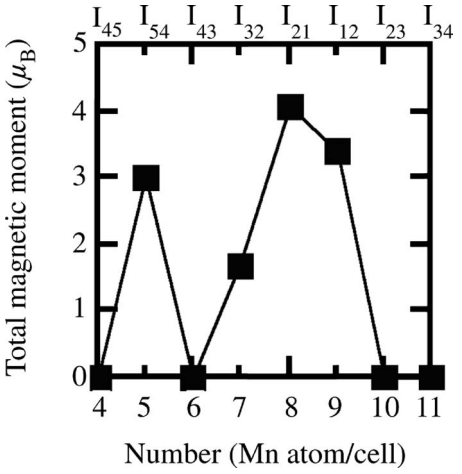


FIG. 6. Total magnetic moment as a function of the number of Mn atoms in a $Mn_4Si_7$ slab for the calculated $Mn_4Si_7/Si(100)$ interface models. The corresponding index of the interface is also shown.

are smaller than those in the bulk. Thus, the $d$ orbitals are localized and ferromagnetism appears. The calculated strong magnetic moment of the interfacial Mn, $\sim 1\mu_B/\mathrm{Mn}$, is rather consistent with that of the interstitial Mn in Si, 3 $\mu_B/\mathrm{Mn}$ (Refs. 25 and 26). These results clearly indicate that the origin of the ferromagnetism of the interface is different from that of the bulk. Therefore, it is expected that the interface is another origin of the ferromagnetism of the nanoparticle materials.

## VI. DISCUSSION OF EXPERIMENT RESULTS

We have found that there are two different mechanisms underlying the ferromagnetism of the $MnSi_{1.7}$ nanoparticles/Si system: One is the VEC change effect due to the stoichiometry change or the charge accumulation assisted by the strain, and the other is the interface effect created by the formation of the interface with the host Si. In this section, we compare our calculated results with our previous experimental results[11] to consider the origin of the ferromagnetism of nanoparticles in Si. We previously reported that the magnetism of nanoparticles/Si system consists of two kinds of ferromagnetisms, the hard and soft magnetic components, and that the hard component offers coercivity values as high as 2500 Oe. First, we discuss the soft component.

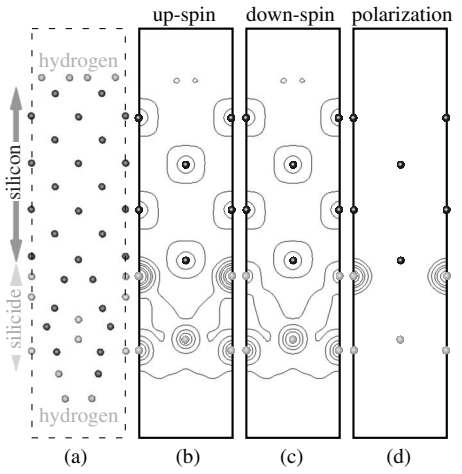


FIG. 7. (a) Atomic structure of the calculated $Mn_4Si_7/Si(100)$ interface model, (b) cross-sectional view of the up-spin state density distribution, (c) cross-sectional view of the down-spin state density distribution, and (d) the difference between the up-spin and the down-spin density distributions. The light and dark circles indicate Mn and Si atoms, respectively. The surface light circles denoted as hydrogen indicate H atoms.

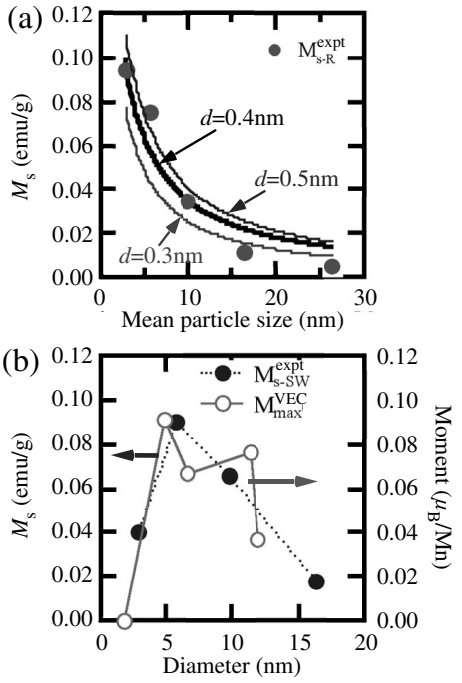


FIG. 8. Experimentally obtained mean particle size dependence of the saturation magnetization and the theoretical curves for (a) the soft and (b) the hard magnetic components. $M_{s-R}^{expt}$ and $M_{s-SW}^{expt}$ are the experimental saturation magnetization plots (Ref. 11) and the solid lines are the theoretical ones. The derivation of the theoretical curves is detailed in the paper.

Figure 8(a) shows the experimentally obtained mean particle size dependence of the saturation magnetization of the soft component and the theoretical curves obtained by the following approach. If we assume that homogeneous magnetization appears in the surface shell region of the nanoparticles, the saturation magnetization $M_{s-R}^{expt}$ should depend on particle radius, $r$, and surface shell thickness, $d$, as $M_{s-R}^{expt} = M_0[1-(1-d/r)^3]$, where $M_0$ is the magnetization per unit area. The thick solid line in Fig. 8(a) is the theoretical curve given when we assume that the surface shell with $d = 0.4$ nm contributes to the magnetism. The thin solid lines correspond to the cases of $d=0.3$ and 0.5 nm. The figure clearly shows the consistency between the experiment and the theory. These values for the shell thickness are well consistent with the thickness of the spin polarized interface region, 0.3–0.5 nm, shown in Sec. V. Therefore, it is suggested that the soft component comes from the nanoparticles surface.

Next, we discuss the hard component. As mentioned in Secs. III and IV, the VEC change could cause the ferromag-

netic ordering of $MnSi_{1.7}$. The stoichiometry and the crystal structures of $MnSi_{1.7}$ nanoparticles are, therefore, very important. It is reported that the phase transformation of the $TiSi_2$ film depends on the film thickness.[41] It follows that the crystal phase of $MnSi_{1.7}$ could also depend on the mean particle size. Figure 8(b) shows the mean particle size dependence of the saturation magnetization of the hard component, $M_{s-SW}^{expt}$, based on the randomly oriented Stoner-Wohlfarth single domain theory with a single coercivity.[42] The figure also shows the maximum magnetic moment, $M_{max}^{VEC}$, dependence on the $c$-axis lengths of the five different phases: $Mn_4Si_7$ ($c=1.75$ nm), $Mn_{11}Si_{19}$ ($c=4.81$ nm), $Mn_{15}Si_{26}$ ($c=6.53$ nm), $Mn_{26}Si_{45}$ ($c=11.34$ nm), and $Mn_{27}Si_{47}$ ($c=11.79$ nm). Both $M_{s-SW}$ and $M_{max}^{VEC}$ have a peak at $\sim 5$ nm as shown in the figure.

Let us assume that the nanoparticle takes one of the $MnSi_{1.7}$ phases when the particle size is similar to the $c$-axis length of the phase. This means that, for example, the nonmagnetic $Mn_4Si_7$ nanoparticle should be dominant and the other phases are rare when the mean particle size is close to the $c$-axis length of $Mn_4Si_7$. When the mean particle size increases and $Mn_{11}Si_{19}$ nanoparticles are formed, the saturation magnetization should increase. When the mean particle size increases further and $Mn_{27}Si_{47}$ nanoparticles are formed, the saturation magnetization might decrease. These relationships can consistently explain the change in saturation magnetization with particle size. In addition, the maximum value of the magnetic moment, $M_{s-SW}^{expt}$ [Fig. 8(b)], which corresponds to $\sim 0.1$ $\mu_B$/Mn, is well consistent with that of the magnetic moment for $MnSi_{1.7}$ and $M_{max}^{VEC}$ derived from the VEC theory.

We note that the phase change cannot, by itself, sufficiently stabilize the ferromagnetism as discussed in Secs. III and IV. That requires strain or charge accumulation. Although we could not experimentally estimate the strength of the strain or the stoichometry change in the nanoparticles, strain should be present due to the lattice mismatch between $MnSi_{1.7}$ and the host Si matrix. Even if extra Mn is doped into the Si as interstitials and $MnSi_{1.7}$ crystals are grown, the tensile strain of $\sim 3-5\%$ should be induced because the volume of $MnSi_{1.7}$ crystal is 0.95–0.97 times that of Si crystal for the same number of Si atoms. It has been also reported that the magnetic properties of MnSi, which is known to be an itinerant magnetic materials, is changed by strain.[43]

The charge accumulation effect is thought to play a similar role. According to Sec. IV, the accumulated charges around $10^{21}-10^{22}$ $cm^{-3}$ is necessary to induce ferromagnetism in $MnSi_{1.7}$ if only the charge accumulation is considered. Charge transfer between the silicide nanoparticles and the host Si matrix might be much smaller. Therefore, the charge accumulation could only modify the value of VEC slightly and is thought to assist the stoichiometry change in the appearance of the ferromagnetism as well as the strain. This implies that the magnetic properties of $MnSi_{1.7}$ nanoparticles could be controlled by the polarity of the host Si matrix, which is consistent with experimental results indicating that $n$-type or $p$-type Si wafers yield different ferromagnetic properties.[6]

We discuss here the coercivities of the soft and the hard components. According to the randomly oriented Stoner-Wohlfarth model, employed in the above discussion,[42] coercivity $H_c$ is given by $H_c=K_u/M_s$, where $K_u$ is the uniaxial magnetic anisotropy constant and $M_s$ is the saturation magnetization. The large measured coercivity $H_c=2500$ Oe is thus thought to come from the hard component with a small magnetic moment $M_s$. This is supported by the fact that the VEC change can induce magnetic moment smaller than 0.1 $\mu_B$/Mn depending on the VEC value. On the other hand, since the interface formation induces the magnetic moment around 1 $\mu_B$/Mn, the coercivity could not be so large and the interface formation is thought to be the source of the soft component.

If we further assume that the effective magnetic anisotropy $K$ of the soft component is similar to that of the hard component, we can roughly estimate the coercivities using the equation $H_c \sim K/M_s$. Using the relation $Kv=25k_BT_B$ [with the Boltzmann constant $k_B$, the averaged particle volume of $v=2.6\times 10^{24}$ $m^{-3}$, and the blocking temperature of $T_B=100$ K (Ref. 11)], the effective anisotropy $K$ of $MnSi_{1.7}$ nanoparticles is estimated to be $K=1\times 10^4$ $J/m^3$—which is reasonably consistent with the generally known values for the uniaxial magnetic anisotropy constant $K_u$. Therefore, the use of the equation $H_c=K_u/M_s$ is thought to be physically valid enough.

The above discussions are, of course, quite rough and somewhat simplistic in clarifying the precise physical origin of the magnetism of $MnSi_{1.7}$ nanoparticles in Si. The magnetic properties are also expected to be impacted by the surface anisotropy and/or the interaction between the interface and the inner moments. The quantized electronic structures in the nanoparticles could also have some effect. However, the above two origins, the VEC change assisted by the strain and the interface formation, can qualitatively well explain the experimental results. We thus believe that our findings are fundamental and very illuminating in understanding the magnetism of $MnSi_{1.7}$ nanoparticles.

## VII. CONCLUSION

The first-principles calculations are conducted to examine the origins of the ferromagnetism of $MnSi_{1.7}$ nanoparticles in Si. The magnetic property of bulk $MnSi_{1.7}$ is affected by stoichiometry, strain, and charge accumulation. Stoichiometry and charge accumulation induce a ferromagnetic state, and strain stabilizes the ferromagnetic state. Moreover, $MnSi_{1.7}$/Si interface formation also causes ferromagnetism, strongly localized at the interface. A comparison to the experimental results of $MnSi_{1.7}$ nanoparticles in Si indicates that these two mechanisms are related to the experimentally derived hard and soft components, respectively.

## ACKNOWLEDGMENTS

The authors thank Kazuyuki Uchida and Akihito Taguchi for their helpful advice. They also thank Hiroshi Yamaguchi for his support throughout this study. A part of this study was supported by JSPS KAKENHI (Grants No. 16206038 and No. 20241036). Some of the calculations were done at the Supercomputer Center, Institute for Solid State Physics, University of Tokyo.

*kages@will.brl.ntt.co.jp


[1] H. Ohno, D. Chiba, F. Matsukura, T. Omiya, E. Abe, T. Dietl, Y. Ohno, and K. Ohtani, Nature (London) **408**, 944 (2000).

[2] A. Oiwa, Y. Mitsumori, R. Moriya, T. Słupinski, and H. Munekata, Phys. Rev. Lett. **88**, 137202 (2002).

[3] K. Takashina, M. Brun, T. Ota, D. K. Maude, A. Fujiwara, Y. Ono, Y. Takahashi, and Y. Hirayama, Phys. Rev. Lett. **99**, 036803 (2007).

[4] Y. Ono, A. Fujiwara, K. Nishiguchi, Y. Takahashi, and H. Inokawa, J. Phys. Chem. Solids **69**, 702 (2008).

[5] R. M. Westervelt, Nature (London) **453**, 166 (2008).

[6] M. Bolduc, C. Awo-Affouda, A. Stollenwerk, M. B. Huang, F. G. Ramos, G. Agnello, and V. P. LaBella, Phys. Rev. B **71**, 033302 (2005).

[7] F. Shimura, *Semiconductor Silicon Crystal Technology* (Academic, San Diego, 1989).

[8] H. H. Woodbury and G. W. Ludwig, Phys. Rev. **117**, 102 (1960).

[9] T. B. Massalski, H. Okamoto, P. R. Subramanian, and L. Kacprzak, *Binary Alloy Phase Diagrams*, 2nd ed. (ASM International, Metals Park, OH, 1992).

[10] S. Zhou, K. Potzger, G. Zhang, A. Mücklich, F. Eichhorn, N. Schell, R. Grötzschel, B. Schmidt, W. Skorupa, M. Helm, J. Fassbender, and D. Geiger, Phys. Rev. B **75**, 085203 (2007).

[11] S. Yabuuchi, Y. Ono, M. Nagase, H. Kageshima, A. Fujiwara, and E. Ohta, Jpn. J. Appl. Phys. **47**, 4487 (2008).

[12] H. Nowotny, F. Benesovsky, and C. Brukl, Monatsch. Chem. **92**, 193 (1961).

[13] B. G. Hyde and S. Andersson, *Inorganic Crystal Structures* (Wiley, New York, 1989).

[14] O. Schwomma, H. Nowotny, and A. Wittman, Monatsch. Chem. **94**, 681 (1963).

[15] S. Schwomma, Y. Preisinger, M. Nowotny, and E. Wittman, Monatsch. Chem. **95**, 1527 (1964).

[16] H. W. Knott, M. H. Mueller, and L. Heaton, Acta Crystallogr. **23**, 549 (1967).

[17] G. Zwilling and H. Nowotny, Monatsch. Chem. **104**, 668 (1973).

[18] H. Q. Ye and S. Amelincks, J. Solid State Chem. **61**, 8 (1986).

[19] P. Villars and L. D. Calvert, *Peason's Handbook of Crystallographic Data for Intermetallic Phases*, 2nd ed. (ASM International, Metals Park, OH, 1991).

[20] U. Gottlieb, A. Sulpice, B. Lambert-Andron, and O. Laborde, J. Alloys Compd. **361**, 13 (2003).

[21] Y. Imai, M. Mukaida, and T. Tsunoda, Intermetallics **8**, 381 (2000).

[22] Y. Imai and A. Watanabe, Intermetallics **13**, 233 (2005).

[23] D. B. Migas, V. L. Shaposhnikov, A. B. Filonov, V. E. Borisenko, and N. N. Dorozhkin, Phys. Rev. B **77**, 075205 (2008).

[24] T. Nakajima and J. Schelten, J. Magn. Magn. Mater. **21**, 157 (1980).

[25] S. Yabuuchi, E. Ohta, H. Kageshima, and A. Taguchi, Physica B (Amsterdam) **376-377**, 672 (2006).

[26] S. Yabuuchi, E. Ohta, and H. Kageshima, Jpn. J. Appl. Phys. **47**, 2630 (2008).

[27] J. P. Perdew, K. Burke, and M. Ernzerhof, Phys. Rev. Lett. **77**, 3865 (1996).

[28] D. Vanderbilt, Phys. Rev. B **41**, 7892 (1990).

[29] K. Laasonen, A. Pasquarello, R. Car, C. Lee, and D. Vanderbilt, Phys. Rev. B **47**, 10142 (1993).

[30] N. Troullier and J. L. Martins, Phys. Rev. B **43**, 1993 (1991).

[31] J. Yamauchi, M. Tsukada, S. Watanabe, and O. Sugino, Phys. Rev. B **54**, 5586 (1996).

[32] M. Tsukada *et al.*, *Computer Program Package TAPP (Tokyo Ab-initio Program Package)* (University of Tokyo, Tokyo, Japan, 1983–2008).

[33] H. Kageshima and K. Shiraishi, Phys. Rev. B **56**, 14985 (1997).

[34] O. Nakanishi, A. Yanase, and A. Hasegawa, J. Magn. Magn. Mater. **15-18**, 879 (1980).

[35] H. Yamada and K. Terao, Phys. Rev. B **59**, 9342 (1999).

[36] W. Jeitschko and E. Parthe, Acta Crystallogr. **22**, 417 (1967).

[37] D. C. Fredrickson, S. Lee, R. Hoffmann, and J. Lin, Inorg. Chem. **43**, 6151 (2004).

[38] D. C. Fredrickson, S. Lee, and R. Hoffmann, Inorg. Chem. **43**, 6159 (2004).

[39] E. C. Stoner, Proc. R. Soc. London **A165**, 372 (1938).

[40] J. Kanamori, Prog. Theor. Phys. **30**, 275 (1963).

[41] N. S. Parekh, H. Roede, A. A. Bos, A. G. M. Jonkers, and R. D. J. Verhaar, J. Magn. Magn. Mater. **38**, 88 (1991).

[42] E. C. Stoner and E. P. Wohlfarth, IEEE Trans. Magn. **27**, 3475 (1991).

[43] C. Pfleiderer, S. R. Julian, and G. G. Lonzarich, Nature (London) **414**, 427 (2001).